EFFECT OF MOISTURE ABSORPTION ON THE MICROMECHANICAL BEHAVIOR OF CARBON FIBER-EPOXY MATRIX COMPOSITES

Javier I. Cauich-Cupul, Alex Valadez-González, Emilio Pérez-Pacheco and Pedro J. Herrera-Franco

Centro de Investigación Científica de Yucatán A. C., Unidad de Materiales
Calle 43 # 130 Col. Chuburná de Hidalgo, C. P. 97200, Mérida Yucatán México
Email: pherrera@cicy.mx

Keywords: *Moisture absorption, fiber-matrix interface, load-transfer capability*

Abstract

The effect of moisture uptake in epoxy matrix/IM7-carbon-fiber composite was studied in controlled humidity environments. The detrimental effect of moisture uptake on the mechanical properties of the matrix, and its deterioration is attributed to a decrease of its Glass transition temperature. The quality of the fiber-matrix interface was assessed using the single fiber fragmentation test and the fiber-fragment length, considered as an indicator of interfacial quality. The fiber fragment lengths were measured using an optical observation system and the results compared to measurements with an acoustic emissions technique. In order to use the second technique, the speed of propagation of an acoustic wave in the material was determined. Excellent agreement between the two techniques was obtained.

Also, a micromechanical model was used to better understand the observed fiber-fragment lengths. The role of moisture uptake swelling of the matrix on the residual stresses is considered to be important when considering the effect deterioration of interfacial shear properties. Both the contribution of the radial stresses and the mechanical component of fiber-matrix adhesion are seen to decrease rapidly for higher moisture contents in the matrix and/or interface.

1 General Introduction

There exists experimental evidence about the degradation of organic type matrices and of the fiber-matrix interfase because of the absorption of moisture [1]. Water absorption in a polymer, is generally accompanied by a volumetric expansion (swelling) that modifies the state of residual stresses in the composite material. This swelling could be attributed to factors such as: (a) The hydrophobic character of the engineering fibers [2]; (b) to the difference of physico-chemical and mechanical properties between fiber and matrix [3]; (c) to a plasticization of the composite, evidenced by its softening and a decrease of its glass transition temperature (T_g) [1, 4]. One of the effects of water absorption is the degradation of the interfacial region between the fiber and the matrix (interphase) by hydrolysis [5] and chemical attack that results in a reduction of the stress transfer between fiber and matrix [6]. Drzal et al demonstrated that the interface in a carbon fiber-epoxy matrix composite material is degraded by moisture and that such degradation has both reversible and irreversible effects, depending on the temperature of hygrothermal exposure, the applied mechanical stress and the type of surface treatment on the fiber.
On the other hand, silane-coupling agents posses organic functional groups that can react with a second functional group of the matrix, forming an inorganic layer with a coupling effect with the fiber. These materials are capable of improving the interaction between the fiber and the matrix, improving the interfacial shear strength and consequently, the mechanical properties of the composite material exposed to either, humid or dry environments. The experimental methods used in the last few years to characterize the interphase in composite materials have focused on the determination of the level of adhesion between the fiber and the matrix and on the interfacial failure modes. Mechanically, the interphase has been characterized as a function of a single parameter: the interfacial shear strength between fiber and matrix.
The method used for the determination of the interfacial shear strength is the single fiber

fragmentation test (SFFT) depicted in figure 1. Traditionally, this fragmentation process is observed and analyzed from the measurement of the final fiber fragment length by optical methods. A second alternative that has been used to determine the fiber fragment lengths is the acoustic emissions technique. This technique offers the advantage over the optical method that it can be used even with opaque matrices, where the points of rupture of the fibers are not visible and direct observation is not possible [8].

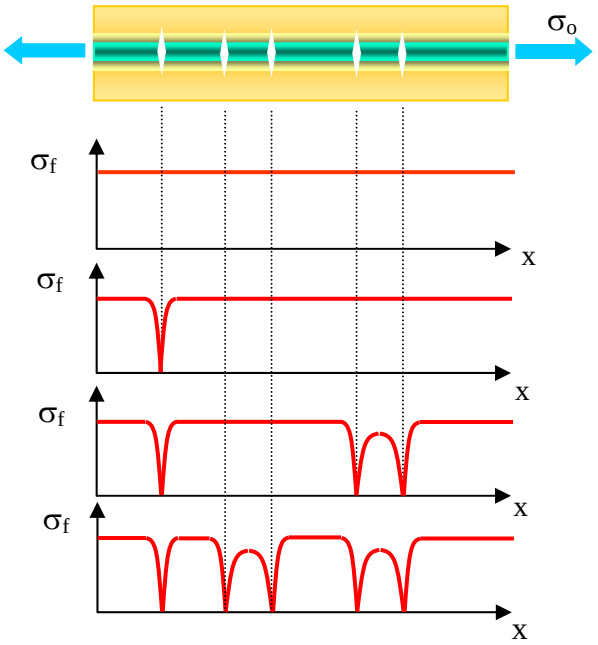

Figure 1. Single fiber fragmentation process

The acoustic emissions technique is based on the fact that when a material is stressed, micro failures in the form of cracks or voids produce a change in geometry and this change leads to a change in the strain of energy. The strain energy changes and the sudden movement produce a stress wave that propagates through the material. When the applied stress increases, many of these emissions are generated. The stress wave propagation is recorded using a highly sensitive piezoelectric sensor, and the signals from one or more sensors are amplified and measured for their interpretation [9, 10]. In the single fiber fragmentation test, failure of the embedded fiber will produce a sudden change in geometry also resulting on the generation of acoustic-wave propagation through the specimen. The fiber fragment length measurement by the acoustic emissions technique is based on the measurement of the speed of propagation of the signal as an acoustic wave through the medium. Such speed could be influenced by geometrical parameters, the frequency of the emitted signal, as well as the deformation of the material. The acoustic emission signal containing detailed information can be detected by one or more sensors and can be used to locate the fiber fragment lengths.

In this paper, the effect of moisture absorption in a matrix and/or interphase on the level of fiber matrix adhesion is studied for three different levels of adhesion. The measurements were performed using the single fiber fragmentation test complemented by optical methods and acoustic emission techniques for the measurement of fiber-fragment lengths.

2. Materials and experimental methods

An amine-epoxy matrix system was selected for this study. A difunctional epoxy, Diglycidil ether of bisphenol A, DGEBA (Epon 828, Shell Chemical Co), was processed at stoichiometric conditions (14.5 phr methaphenilene diamine, mPDA, Aldrich Chemical Co) for the single fiber fragmentation test coupons for 2 h at 75°C and 2 h at 125°C.

Intermediate modulus carbon fibers, type IM7 from Excel Corp an as a coupling agent, 3-glycidoxy propyltrimethoxysilane, Z6040 from Dow Corning were used.

2.1 Fiber surface treatments

The single fiber fragmentation test coupons were prepared using the IM7 carbon fiber with three different surface treatments. The nomenclature used for each fiber surface treatment is the following: (1) IM7, refers to the carbon fiber, “as received”; (2) IM7+Silane, refers to the IM7 fiber whose commercial sizing was removed and treated with the selected silane coupling agent, and (3) IM7+HNO3+Silane, refers to the IM7 fiber, but treated with nitric acid and the silane coupling agent after removal of the commercial sizing.

For the removal of the commercial sizing, the fibers were immersed and refluxed in methyl-ethyl ketone in a Kettle reactor during 12 hours. Afterwards, they were washed with acetone and then, with distilled water. Finally, they were dried in an oven at 120° C for 24 hours.

For the silane coupling agent surface treatment, distilled water and methanol were first thoroughly mixed (50 % v/v) and the pH of the solution measured and adjusted to 4.5 using a diluted solution of acetic acid. Then, the silane coupling agent was added to a concentration of 0.1 % (w/w) and agitated

for two additional hours. Then the fibers were immersed in the solution for one hour, and then hey were dried in an oven at 120° C during one hour.
The nitric acid fiber surface treatment was applied to the carbon fibers after removal of the commercial sizing. The fibers were immersed in the acid (70% purity) and refluxed for 6 hours in a Kettle reactor. Afterwards the fibers were washed in distilled water and refluxed for two hours in the reactor to remove any traces of the acid and then, they were dried during in an oven at 120° C for two hours.

2.2 SFFT coupon preparation

Epoxy-matrix test coupons for the single-fiber fragmentation test were fabricated by a casting method with the aid of a silicone room temperature vulcanizing eight-cavity mold. Standard ASTM 50.8 mm long dogbone specimen cavities with a 3.175 mm wide by 1.587 mm thick by 25.40 mm long gauge section are molded into a 76.20 x 203.20 x 12.70 mm silicone piece. Single fibers approximately 150 mm in length are selected by hand from a fiber bundle. Single filaments are carefully separated from the fiber tow without touching the fibers, except at the ends. Once selected, a filament was mounted in the mold and held in place with a small amount of rubber cement at the end of the sprue. The assembly was transferred to an oven (Squaroid, Model 3608-5, for 2 hours at 75°C and 2 hours at 125°C) until the curing cycle was completed. The specimens were tested in uniaxial tension using a microstraining machine (MINIMAT) capable of applying enough load to the tensile coupon and fitted with a 1000 N load cell. The samples were tested using a cross-head speed of 0.02 mm/min. The load was applied and the inspection of the fiber fragmentation processed was assessed every 0.5 mm elongation intervals by counting the number of fragments. This processed was repeated until the number of fiber fragments did not increase with an increase of the applied load. At this point the test was stopped and the resulting fiber fragments were measured using an optical caliper Image XR2000. The image of the fibers was magnified using a 50x Olympus microscope objective lens (Neo Plan50) fitted to a TV camera which was connected to a TV monitor. In order to asses the failure process, a transmitted light polarizing microscope was configured such that there was one polarizer below and one above the test coupon for observation of the photoelastic pattern evolution as a result of the induced birefringence in the matrix.

2.3 Moisture conditioning

The samples were conditioned to several relative humidity controlled environments **(**25%, 55% y 95%) at a constant temperature of 25° C, until ready for the mechanical and interfacial characterization. Air-tight sealed glass chambers were used as conditioning chambers. The different relative humidity environment chambers were obtained using several saturated salts. These salts were selected to obtain the different relative humidity atmospheres according to ASTM E104-51 and E104-85 standards, [11 and 12]. A digital hygrometer was place inside each chamber in order to measure and continuously monitor the temperature and relative humidity inside each chamber.
The weight gain of the test coupons after exposure to the selected relative humidity environments was measured as a function of time. The humidity content was estimated using the following equation [13, 14]:

$$M = \frac{M_W - M_d}{M_d} x100\% \qquad \textbf{(1)}$$

Where M is the amount of gained humidity, M_w is the weight of the wet sample and M_d is the weight of the dry sample.

2.4 Determination of the speed of propagation of the acoustic signal

The speed of propagation of the acoustic signal in the epoxy samples, before and after moisture exposure was measured utilizing two piezoelectric transducers (see sensors 1 and 2 in figure 2). Each transducer with an effective area of contact equal to 17.795 mm^2 was affixed to the tensile test coupon and to insure good contact, vacuum silicon grease was used. A notch, 0.5 mm deep was cut on one side of the coupon as a crack initiator. These two piezoelectric sensors were located at known distances from the notch. Sensor one was located at 4.88 mm from the notch and sensor two at 9.88 mm.

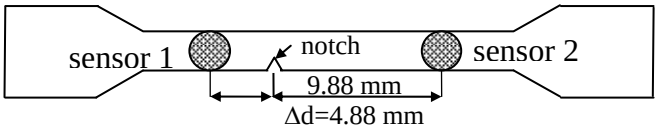

Figura 2. Test coupon for the determination of the speed of propagation of the acoustic signal.

A tensile load was applied to the test coupon using a mini tensile testing device (MINIMAT) equipped with a load cell of 1000 N. The cross-head speed was fixed at 0.02 mm/min. Upon crack initiation, the stress wave propagating as an acoustic signal was recorded and analyzed using commercial software called MITRA™. The difference in the time of arrival (Δt) of the acoustic signal to each of the sensors, and corresponding to the first event of crack growth was recorded (see figures 3 and 4). Then the speed of propagation was calculated using the equation:

$$V = \frac{\Delta d}{\Delta t} \qquad (2)$$

Where V is the average speed of propagation of the acoustic signal, Δd is the difference of distance between the location of the sensors and the notch in the test coupon. This procedure was repeated for the test coupons conditioned at the selected relative humidity.

2.5 Determination of Young´s modulus using acoustic signals

The speed of propagation of a wave in a medium is a function of the properties of the material itself and geometrical parameters, dominating frequency of the emitted signal, and most important, the deformation produced in the material, that is:

$$\sigma_{xx} = \left(\frac{E}{c_o}\right)\frac{\partial u}{\partial t} = \rho c_o \frac{\partial u}{\partial t} \quad \acute{o} \qquad E = \frac{\sigma^2}{V^2}\rho \quad (3)$$

This equation shows that there exists a linear relationship between the stress at any point in the material and the speed of the particle, being this relationship between them, the corresponding impedance, ρc_o.

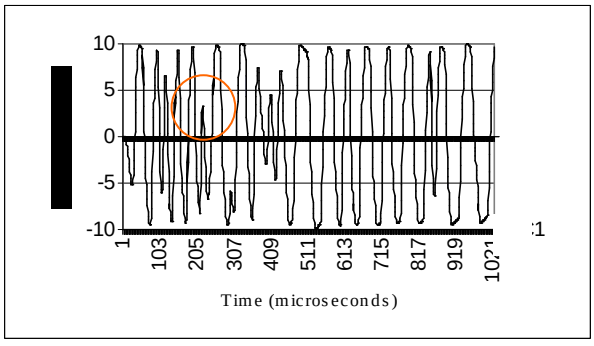

Figure 3. Graph of signal amplitude versus time of arrival to sensor 1

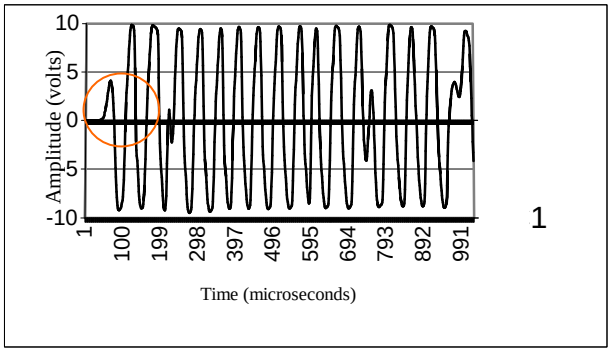

Figure 4. Graph of signal amplitude versus time of arrival to sensor 2.

2.6 Measurement of fiber fragment length using acoustic emissions.

The fiber fragment lengths while performing the single fiber fragmentation test were also measured using the acoustic emissions arising from the fiber fracture, and both the interfacial crack growth and the matrix-crack growth. The acoustic emissions were detected using the same two piezoelectric transducers (see figure 5). Each transducer with an effective area of contact equal to 17.795 mm^2 was affixed to the tensile test coupon and to insure good contact, vacuum silicon grease was used. The distance between transducers was fixed at 14.76 mm using a template especially built to accurately position them always at the same distance.

A tensile load was applied to the test coupon using a mini tensile testing device (MINIMAT) equipped with a load cell of 1000 N.

The cross-head speed was fixed at 0.02 mm/min.

Upon crack initiation, the stress wave propagating as

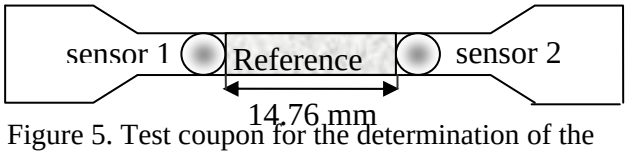

Figure 5. Test coupon for the determination of the fiber fragment lengths using the acoustic emissions technique.

an acoustic signal was recorded and analyzed using commercial software called MITRA™. A threshold value of 40 dB was used to isolate the high sensitivity transducers from external noise. The acoustic signals were pre-amplified using preamplifiers whose gain was also set to 40 dB. A frequency range from 10 KHz a 1200 KHz was used in the test and the speed of event detection was set to 10 Mhz in a synchronized mode. A simple algorithm

incorporating the average wave speed in the epoxy (or any other matrix), the distance between the two receiving transducers, the offset distance between one specific receiving transducer and the fixed grip, time intervals and the corresponding strains was used to obtain the location of the fiber breaks, the fiber fragment lengths and fiber aspect ratios. In the case of the acoustic emissions fiber-fragment measurement, the fragmentation process was monitored only as a function of the acoustic signals being monitored, that is, once the load was applied, the test was ended when no more signal were being registered by the system. The strain in the sample was also continuously monitored to avoid sample fracture.

3. Results and discussion

Figure 6 shows isotherms of absorbed moisture as a function of time for the different relative humidity atmospheres. For the 25 % RH, the amount of gained weight stabilizes at approximately 0.15% after 90 days of exposure. For the 55% RH, a larger amount of moisture is gained during the first 20 days and then it stabilizes at a maximum of 1% after 90 days of exposure. For the 95% RH, the maximum amount of absorbed water of approximately a 2% was achieved after 290 days of exposure. It was observed that the moisture absorption rate was high at the beginning of the exposure of the samples, especially during the first 20 days; afterwards, the absorption rate slowly decreased until 90 days of exposure and then it stabilized to a maximum of 1%. Only for the 95% RH environment, the absorption rate rapidly increased during the first 20 days and then it stabilized to a moisture gain of approximately 2%, after 90 days.

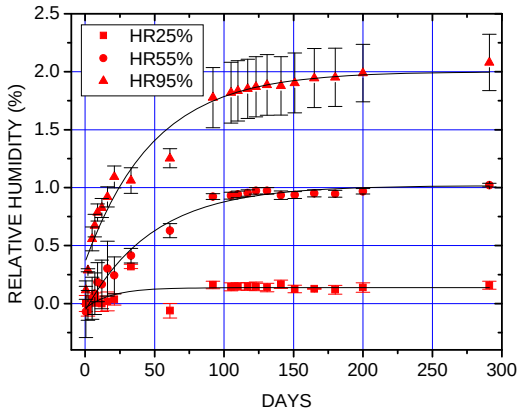

Figure 6. Isotherms of moisture absorption for the epoxy resin.

Figures 7 and 8 show the tensile strength and the elastic modulus of the epoxy matrix as a function of absorbed moisture during 290 days respectively. The decrease of the resin tensile strength notoriously decreases when the amount of absorbed moisture increases. For the highest moisture gain, such tensile strength decreases from 85 MPa to 65 MPa, that is, a loss of approximately 23.5 %. As shown in figure 7, the decrease of the matrix rigidity of approximately 16.4% is notorious after moisture absorption of 0.1 %. Such rate of change is high during the first 20 days of exposure, and then it slowly decreases with higher moisture gain.

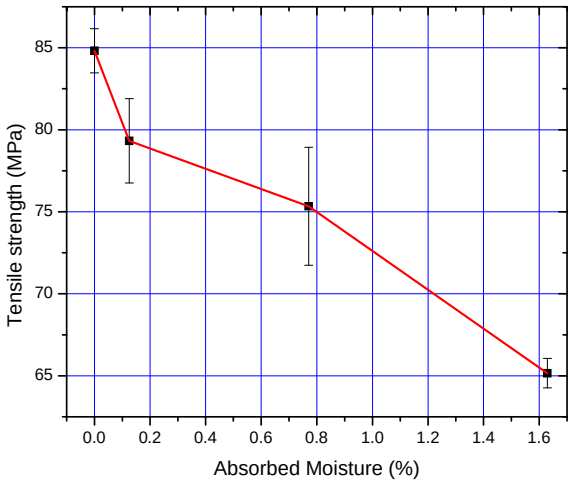

Figure 7. Tensile strength as a function of absorbed moisture.

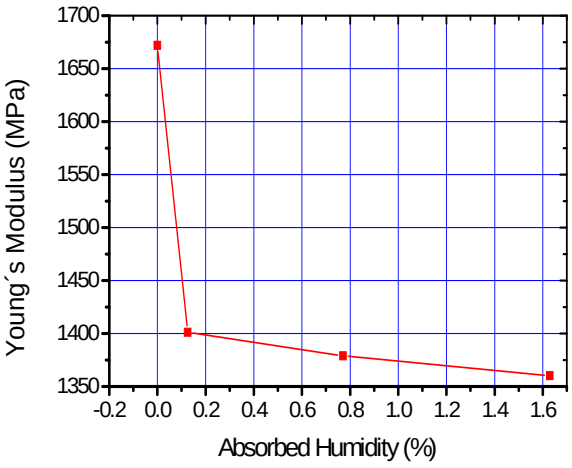

Figure 8. Young's modulus of the epoxy matrix as a function of absorbed moisture.

The effect of moisture absorption on the mechanical properties of the polymer is attributed to a plasticization as evidenced by a reduction of its glass transition temperature Tg [4, 5]. The degradation of the mechanical properties of epoxy polymers due to

moisture absorption is associated to the plasticization and to a micromechanical damage induced by the absorbed moisture [16]. The decrease of the properties caused by the interactions between the polymer and the absorbed water is a rapid and powerful phenomenon with an apparent stability during the first stage of moisture diffusion. Afterwards, the tendency of the polymer network to absorb moisture decreases and a relative stabilization is observed [17]. As mentioned before, the speed of propagation of an acoustic signal in a medium is a function of the physico-chemical properties of the material. As shown in figure 9, for an epoxy resin after exposure at a 95% RH, a 2% moisture absorption results in a decrease of acoustic signal propagation speed of approximately a 22.72% as compared to a 0% moisture absorption. Then, the decrease of the stiffness of the material results in a damping of the acoustic signal as it travels in the material. This damping should be related to the viscoelastic behavior of the matrix, since its Tg is decreasing and its loss modulus is increasing.

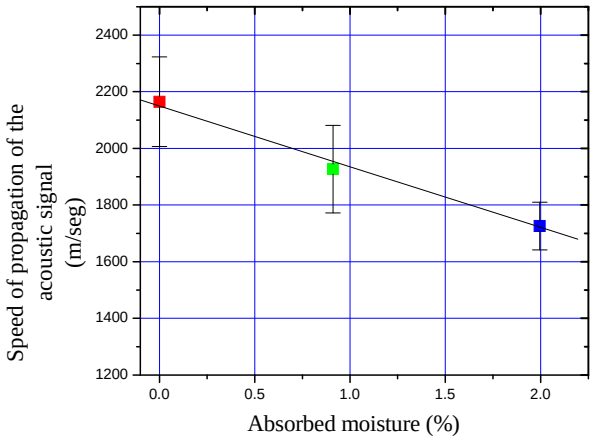

Figure 9. Speed of propagation of the acoustic signal as a function of absorbed moisture.

The fiber-critical length is very important for the calculation of the interfacial shear strength, especially when studying the degradation caused by hygrothermal exposures of the composite. Such fiber-critical length is considered an indicator of fiber-matrix adhesion level in the composite. Therefore, the interpretation of the change in the fiber critical length as a function of absorbed moisture clearly shows how this fiber-matrix adhesion is deteriorating because of moisture diffusion in the composite. As shown in figure 10, there is notorious increment of the average L_c for the untreated carbon fiber (IM7) with increasing moisture content. The fiber-fragment length rate of change with absorbed moisture follows al three linear stages. The first stage is noticed up to a moisture content of approximately 0.25%, and the second up to 0.85%. The third stage for higher moisture contents. Longer fragments were measured with higher amounts of absorbed moisture. However, when the fiber-matrix adhesion is changed, either with the new silane treatment or the nitric acid activated and silane treated fiber, two different stages of fiber-fragment length as a function of absorbed moisture are observed. There is a high rate of change up to a 0.5% of absorbed moisture and afterwards, no notorious change is observed, even for high moisture contents in the matrix. No notorious difference is observed in the critical length behavior when the fiber is treated with nitric acid. Similar trends of the change of average critical length was noticed when it was measured using the acoustic emissions technique (see figure11).

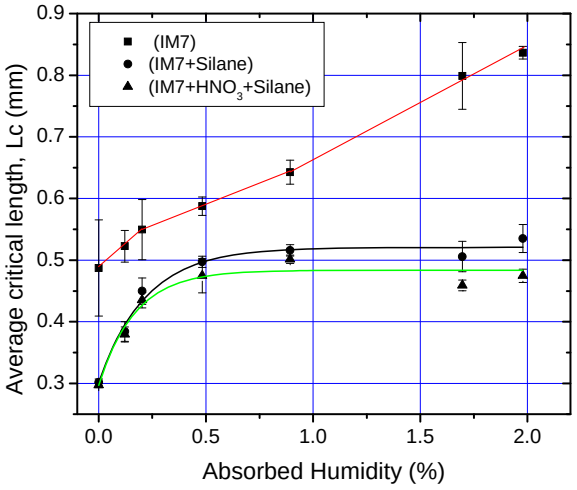

Figure 10. Average fiber critical length as a function of absorbed moisture as measured by the optical method.

Swelling is a specific response to moisture diffusion in epoxy resins or composites based on them [19-21]. It is very important in both composites and adhesive joints, because it can significantly affect mechanical behavior by build-up of residual stress at and near interfaces.

Hygroscopic swelling is mechanically similar to thermal expansion in that both are physical phenomena involving molecules equilibrating a larger distance apart as a result of temperature increase and moisture absorption, respectively.

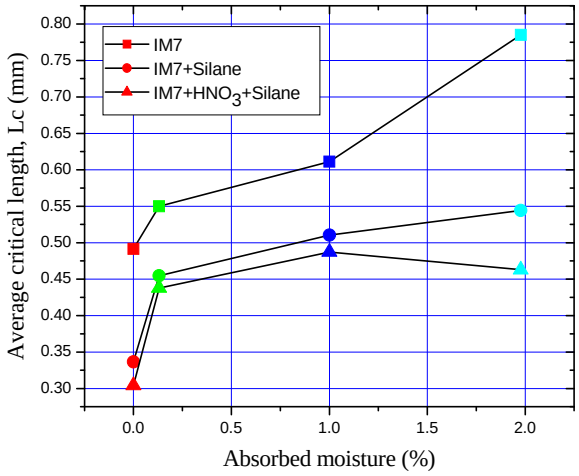

Figure 11. Average fiber critical length as a function of absorbed moisture as measured by the acoustic emissions method.

In both, the magnitudes of expansion, ε_T and ε_M are given by:

$$\varepsilon_T = \alpha \Delta T \qquad \varepsilon_M = \beta \Delta M \qquad (4)$$

Where α and β are the coefficients of thermal and moisture expansion coefficients respectively, ΔT and ΔM are temperature and moisture gradients respectively.

Whitney and Drzal [22] proposed a theoretical model to predict the stresses in a system consisting of a broken fiber surrounded by an unbounded matrix. The model (Figure 12) is based on the superposition of the solutions to two axisymmetric problems, an exact far-field solution and an approximate transient solution. The approximate solution is based on the knowledge of the basic stress distribution near the end of the broken fiber, represented by a decaying exponential function multiplied by a polynomial. Equilibrium equations and the boundary conditions of classical elasticity theory are exactly satisfied throughout the fiber and matrix, while compatibility of displacements is only partially satisfied. The far-field solution away from the broken fiber end satisfies all the equations of elasticity. The model also includes the effects of expansional hygrothermal strains and considers orthotropic fibers of the transversely isotropic class.

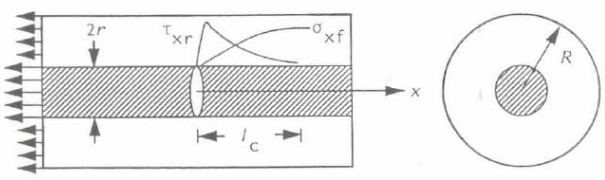

Figure 12. Micromechanical model for the single fiber fragmentation process.

A relationship is obtained for the axial normal stress σ_x in the fibre (see Fig. 11):

$$\sigma_x = \left[1 - (4.75\bar{x} + 1)e^{-4.75\bar{x}}\right] C_1 \varepsilon_0 \qquad (5)$$

where $\bar{x} = x/l_c$, ε_0 is the applied far-field strain and C_1 is a constant dependent on material properties, thermal strains and the applied far-field strain. It can be noticed that σ_x is independent of the fiber radius. The critical length 1_c is defined such that the axial stress recovers 95% of its far-field value, that is:

$$\sigma_x(l_c) = 0.95 C_1 \varepsilon_0 \qquad (6)$$

The interfacial shear stress is given by the expression:

$$\tau_{xR}(\bar{x}, r) = -4.75 \mu C_1 \varepsilon_0 \bar{x} e^{-4.75\bar{x}} \qquad (7)$$

where ($0 \leqq r \leqq R$).

$$\mu = \sqrt{\frac{G_m}{E_{1f} - 4\nu_{12f} G_m}} \qquad (8)$$

E_{lf} denotes the axial elastic modulus of the fiber, whereas v_{12f} is the longitudinal Poisson's ratio of the fiber, determined by measuring the radial contraction under an axial tensile load in the fiber axis direction, and G_m, denotes the matrix shear modulus. It should be noted that the negative sign in the expression for the shear stress is introduced to be consistent with the definition of an interfacial shear stress in classical elasticity theory. The radial stress at the interface is given by:

$$\sigma_r(\bar{x}, r) = \left[C_2 + \mu^2 C_1 (4.75\bar{x} - 1) e^{-4.75\bar{x}}\right] \varepsilon_0 \qquad (9)$$

Constants C_2 and C_1 are dependent on material properties, thermal strains and the applied far-field strain. Numerical results are normalized by σ_0, which represents the far-field fiber stress in the absence of expansional strains. In particular:

$$\sigma_0 = C_3 \varepsilon_0 \qquad (10)$$

The constants C_1, C_2 and C_3 are given by:

$$C_1 = E_{1f}\left(1-\frac{\bar{\varepsilon}_{1f}}{\varepsilon_0}\right)+ \frac{4K_f G_m \nu_{12f}}{\left(K_f+G_m\right)}\left\{\left(\nu_{12f}-\nu_m\right)+\frac{\left[\left(1+\nu_m\right)\bar{\varepsilon}_m-2\bar{\varepsilon}_{2f}-\nu_{12f}\bar{\varepsilon}_{1f}\right]}{\varepsilon_0}\right\} \quad (11)$$

$$C_2 = \frac{2K_f G_m}{\left(K_f+G_m\right)}\left\{\left(\nu_{12f}-\nu_m\right)+\frac{\left[\left(1+\nu_m\right)\bar{\varepsilon}_m-2\bar{\varepsilon}_{2f}-\nu_{12f}\bar{\varepsilon}_{1f}\right]}{\varepsilon_0}\right\} \quad (12)$$

$$C_3 = E_{1f}+\frac{4K_f G_m \nu_{12f}\left(\nu_{12f}-\nu_m\right)}{\left(K_f+G_m\right)} \quad (13)$$

and

$$K_f = \frac{E_f}{2\left(2-\frac{E_{2f}}{2G_{2f}}-\frac{2\nu_{12f}^2 E_{2f}}{E_{1f}}\right)} \quad (14)$$

Where the thermal strains are indicated by overbars, and E_{2f}, G_{2f} and K_f are the radial elastic modulus, the shear modulus in the plane of the cross-section and the plane-strain bulk modulus of the fiber, respectively.

The material properties used are shown in Table 2. The reference moisture value used was a 25% RH and is referred to as 0%.

Table 1. Fiber and matrix material properties

Property	Epoxy resin			IM7
	0%	0.9%	2%	
E_1 (GPa)	1.435	1.318	1.303	241
E_2(GPa)	1.435	1.318	1.303	21
ν_{12}	0.35	0.35	0.35	0.25
G23 (GPa)	0.53			8.3
$\alpha 1$ (10^{-6} °C^{-1})	68			-11
$\beta 1$ (10^{-6} %M^{-1})	0.33			-

As seen in figure 13, the moisture uptake influences the stress distribution along the fiber-matrix interface. For the untreated fiber, the maximum axial stress is achieved a point located farther away from the point of fiber break. Thus, a longer fiber fragment length could be expected. In the case of the silane treated fiber, the maximum axial stress occurs at a point located closer to the fiber break. Here, a shorter fiber fragment could be expected. This is consistent with the measured fiber fragment lengths measured experimentally.

Also, a higher shear interfacial shear stress is observed for the silane-treated fiber, and the distribution along the fiber fragment decreases more rapidly at points located far away from the break (see figure 14).

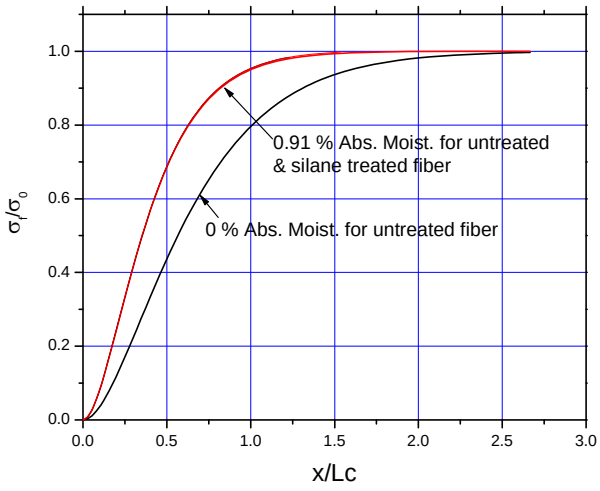

Figure 13. Interfacial fiber axial stress distribution for untreated & silane treated fiber for two different relative humidity environments

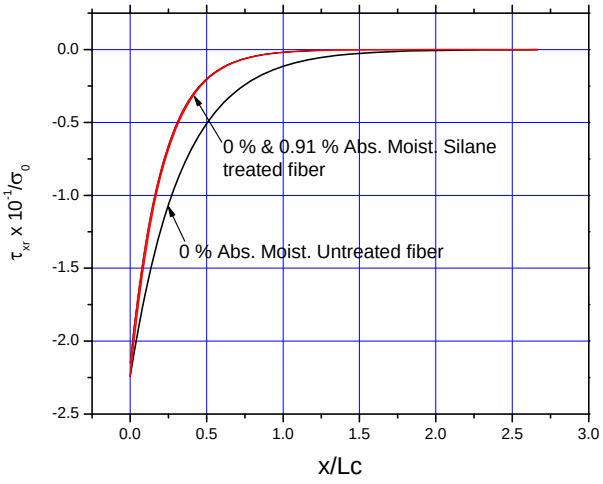

Figure 14. Interfacial shear stress distribution for untreated & silane treated fiber for two different relative humidity environments

Furthermore, swelling due to moisture uptake can be used to explain the fiber-matrix interface degradation. For the 0 % moisture uptake, the residual stress in the radial arising from both curing and thermal coefficients of expansion of direction between fiber and matrix and the expansional strains due to moisture uptake decrease considerably for higher moisture contents.

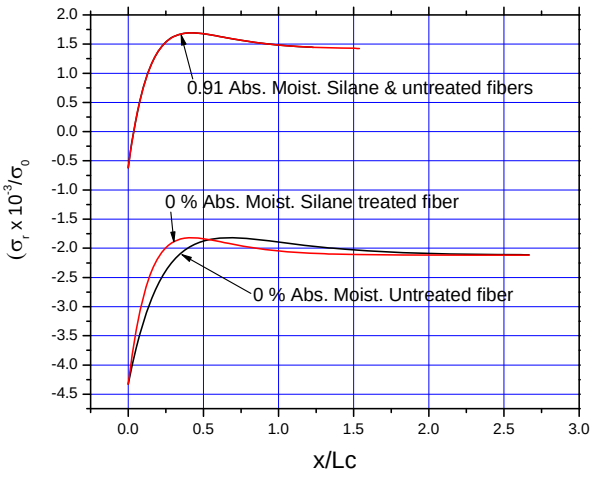

Figure 15. Interfacial radial Interfacial shear stress distribution for untreated & silane treated fiber for two different relative humidity environments stress distribution for untreated & silane treated fiber for two different relative humidity environments

Both thermal and moisture strains decrease and this should result in a reduction of the radial stress component (shown in figure 15), which is considered to contribute to the frictional interfacial shear stress component. In the case of the untreated fiber, since no physico-chemical interactions exist between fiber and matrix, such mechanical component to adhesion is important. In the case of the silane treated fiber, the existence of covalent bonds between the fiber and matrix explain the behavior of the constant fiber fragment lengths, even at high moisture contents.

4. Conclusions

Moisture uptake in epoxy/carbon-fiber composite results in a detrimental effect on the mechanical properties of the matrix, and this deterioration is attributed to a decrease of its Glass transition temperature. The quality of the fiber-matrix interface was assessed using the single fiber fragmentation test and the fiber-fragment length, considered as an indicator of interfacial quality indicated a continuous deteriorating effect of moisture uptake. The fiber fragment lengths were measured using an optical observation system and the results compared to an acoustic emissions technique. In order to use the second technique, the speed of propagation of an acoustic wave in the material was determined. Excellent agreement between the two techniques was obtained. Also, a micromechanical model was used to explain the observed fiber-fragment lengths. The role of moisture uptake swelling of the matrix on the residual stresses is considered to be important when considering the effect deterioration of interfacial shear properties. The contribution of the radial stresses is seen to decrease rapidly and the mechanical component of fiber-matrix adhesion also decrease rapidly for higher moisture contents in the matrix and/or interface.

References

1. G. Z. Xiao, M.E.R. Shanahan, “Water Absorption and Desorption in an Epoxy Resin with Degradation”, *Journal of Polymer Science: Part B: Polymer Physics*, Vol. 35, 2659-2670 (1997).
2. D. P., Pomies, F. y Carlsson, L.A., "Influence of Water and Accelerated Aging on the Shear and Fracture Properties of Glass/Epoxy”, *J. Appl. Compos. Mater*., Vol. 3, 71-80, (1996).
3. Adams, D.F., "A Micromechanies Analysis of the Influence of the Interface on the Performance of Polymer Matrix Composites", Proc. Of the American Society for Composites, lst. Tech. Conf., Oct. 7-9, 1986, Dayton, OH, Technomic, 207.
4. A. Chateauminois, B. Chabert, J. P. Soulier, y L. Vincent, “Dynamic Mechanical Analysis of Epoxy Composites Plasticized by Water :Artifact and Reality”, *Polymer Composites*, Vol 16, 288-296, (1995).
5. C. L. Soles, F. T. Chang, D. W. Gidley, A. F. Yee, “Contributions of the nanovoid Structure to the Kinetics of Moisture Transport in Epoxy Resins”, *Journal of Polymer Science: Part B: Polymer Physics*, Vol 38, 776-791 (2000).
6. Drzal, L.T., Rich, M.J. y Koenig, M.F. "Adhesion of Graphite Fibers to Epoxy Matrices: III. The effect of Hydrothermal Exposure", *Adhesion*, Vol., 18, 49-56, (1985).
7. C. J. Spragg, y L. T. Drzal, “Fiber, matrix, and Interface Properties”, ASTM STP 1290, (1994).
8. A. N. Netravali, Z.-F. Li, W. H. Sachse, y H. F. Wu, “Acoustic emission Coupled Single-Fiber-Composite Technique (SFC/AE) for the Measurement of Interfacial Shear Strengh of High Performance Fibers in Epoxy”, 3th Conference on Advanced Engineering Fibers and Textile Structure for Composites, NASA Conference Publication 3082, J. D. Buckley, Ed., Hampton, VA, 375-381(1990).
9. J. M. Park, E. M. Chong, Dong-Jin Yoon, y Joon-Hyun Lee, ”Interfacial Properties of Two SIC Fiber-Reinforced Polycarbonate Composites Using the Fragmentation Test and Acoustic Emission”, *Polymer Composites*, Vol. 19, 747-758, (1998).

10. L. E. Nielsen, R. F. Landel, ”Mechanical properties of polymers and composites”, Second edition, revised y expanded, Marcel Dekker, Inc., New York, (1994).
11. “Maintaining Constant Relative Humidity by Means of Aqueous Solutions”, ASTM Designation E 104-85, 32-34, (1985). “Maintaining Constant Relative Humidity by Means of Aqueous Solutions”, American Society for Testing Materials, 1916 Race ST., Philadelphia 3, PA., Book of ASTM Standards, Part 6.
12. J. Mijovic, y King-Fu Lin, “The Effect of Hygrothermal Fatigue on Physical/ Mechanical Properties and Morphology of Neat Epoxy Resin and Graphite/Epoxy Composite”, *Journal of Applied Polymer Sciense*, Vol. 30, 2527-2549, (1985).
13. M. R. Vanlandingham, R. F. Eduljee, J. W. Gillespie, JR., “Moisture Diffusion in Epoxy Systems”, *Journal of Applied Polymer Sciense*, Vol. 71, 787-798, (1999).
14. G. Z. Xiao, M. E. R. Shanahan, “Irreversible Effects of Hygrothermal Aging on DGEBA/DDA Epoxy Resin”, *Journal of Applied Polymer Sciense*, Vol. 69, 363-369, (1998).
15. M. G. Lu, M. J. Shim, S.W. Kim, “Effects of moisture on Properties of Epoxy Molding Compounds”, *Journal of Applied Polymer Sciense*, Vol. 81, 2253-2259, (2001).
16. P. Nogueira, C. Ramirez, A. Torres, M. J. Abad, J. Cano, J. Lopez, I. Lopez-Bueno, L. Barral, “Effect of Water Sorption on the Structure and Mechanical Properties of an Epoxy Resin System”, *Journal of Applied Polymer Sciense*, Vol. 80, 71-80, (2001).
17. V. Rao, y L. T. Drzal, “The Dependence of Interfacial Shear Strength on Matrix and Interphase Properties”, *Polymer Composites*, Vol.12, 48-56, (1991).M. J. Adamson, J. Mater. Sci., 15, 1736 (1980).
18. M. L. Jackson, B. J. Love and S. R. Hebner, J. Mater. Sci., Mater. Electron., 10, 71 (1999).
19. Z. R. Xu and K. H. G. Ashbee, J. Mater. Sci., 29, 394 (1994).
20. L. El-saad, M. I. Darby and B. Yates, J. Mater. Sci., 24, 1653 (1989).
21. P. R. Ebrahimzadeh and D. H.Mcqueen, J. Mater. Sci., 33, 1201 (1998).
22. J. M. Whitney, L. T. Drzal, ”Axisymmetric Stress Distribution Around an Isolated Fiber Fragment. In toughened Composite. ASTM STP 93, (N. J. Johnston ed.) ASTM Philadelphia, PA, pp. 179-196.